Free vibration analysis of 2D FG plates by a meshfree boundary-domain integral equation method

***Y. Yang[1, 2], K.P. Kou[2], V.P. Iu[2], C.C. Lam[2], Ch. Zhang[1]**

[1]Department of Civil Engineering, Faculty of Science and Technology, University of Siegen, Germany
[2]Department of Civil Engineering, Faculty of Science and Technology, University of Macau, Macau, China

*Corresponding author: yangyang.liju@hotmail.com

Abstract

Free vibration of two-dimensional functionally graded plates with an exponential material gradation is analyzed in this paper by a meshfree boundary-domain integral equation method. Based on two-dimensional elasticity theory, boundary-domain integral equations are derived by using elastostatic fundamental solutions. Due to the material inhomogeneity and the inertial effect, two domain integrals emerge in the boundary-domain integral equation formulation. Radial integration method is employed to convert the domain integrals into boundary integrals. A meshfree scheme is achieved through approximating the normalized displacements in the domain integrals by a combination of the radial basis functions and polynomials. Thus, the free vibration problem is reduced to a generalized eigenvalue problem, which involves system matrices with boundary integrals only. By using the present meshfree boundary-domain integral equation method, free vibration of two-dimensional exponentially graded plates with various material gradients, boundary conditions and aspect ratios are investigated, which demonstrates the high convergence, efficiency and accuracy of the present method.

Keywords: free vibration, functionally graded plates, exponential material gradation, boundary element method, meshfree method, boundary-domain integral equations.

Introduction

Functionally graded materials (FGMs) are heterogeneous advanced composite materials, in which the volume fractions of the constituents vary gradually and functionally. It has drawn the attentions of the engineering and scientific communities of various disciplines since the concept was first introduced in 1984. Meanwhile, FGMs bring extraordinary merits of high resistance of temperature gradients, high wear resistance and an increase in strength to weight ratio, which make FGMs having motivated the word-wide research activities.

The determination of the natural frequencies and the mode shapes of a functionally graded (FG) structure is an important and necessary process during the engineering design and development. Thus dynamic analysis of the FG plates plays an indispensable role in the engineering practice. Due to the mathematical complexity, most practical problems of FG plates can be solved only with numerical scheme. Among many numerical methods, the boundary element method (BEM) with its superior efficiency and accuracy has been well established as a powerful method. The dual reciprocity method (DRM) proposed by Nardini and Brebbia (1983) is recognized as one efficient method to treat the dynamic analyses of structures (Wilson et al. 1990) and FGMs (Masataka et al. 2000) in BEM. However, the application of DRM to deal with the domain integrals in the boundary-domain

integral equations requires particular solutions, whose construction is restricted to the approximation functions chosen. Another efficient alternative technique to handle the domain integrals in BEM is the radial integration method (RIM) proposed by Gao (2002). The RIM is based on pure mathematical treatments, and the main advantage of the RIM over the DRM is that the radial basis functions (RBF) can be freely chosen. The RIM has been successfully implemented and applied to elastodynamic problems in anisotropic materials by Albuquerque et al (2003, 2007). A meshless boundary-domain integral equation method for transient thermoelastic analysis has been developed and applied by Ekhlakov et al (2010, 2012), where the Laplace-transform technique is used and the domain integrals are handled by the RIM. In contrast to the above mentioned investigations, few works can be found in literature on the vibration problems of FG plates by using these methods.

In this paper a meshfree boundary-domain integral equation method is presented to analyze the free vibration behaviours of two-dimensional (2D) FG plates. The material properties are assumed to vary continuously according to the exponential law either in longitudinal or in transverse directions. The boundary-domain integral equations are derived based on 2D elastodynamic theory, while the elastostatic fundamental solutions for homogeneous materials are applied. The RIM is applied to transform the domain integrals into boundary integrals. A meshfree scheme is achieved by approximating the normalized displacements in the domain integrals by a combination of the radial basis functions and polynomials in term of the global coordinates. Internal nodes are necessary to increase the accuracy of the solution due to the fact that the correct function approximation requires a rather uniform distribution of nodal points. Then the eigenvalues and eigenvectors can be obtained by solving the generalized eigensystem with only boundary discretization. Numerical examples demonstrate that the present method has high efficiency and accuracy. The main advantages of the present method can be summarized as:

(1) The present method is based on a boundary-domain integral equation formulation. It requires the discretization of the global boundary of the problem domain and some internal nodes, but no domain-like elements.
(2) The present method uses elastostatic fundamental solutions and avoids the complicated complex frequency-domain dynamic fundamental solutions.
(3) The present method for computing the eigensolutions is quite robust. No instability and spurious eigenvalues are observed by using the method, which is a critical issue in real valued BEM to analyze eigenvalue problems.
(4) Numerical examples for free vibration analyses of 2D FG plates with various material gradation directions, gradient parameters, aspect ratios, and boundary conditions show the fast convergence, high efficiency and accuracy of the present method. In addition, the present method is easy to implement and very flexible for free vibration analyses of 2D FG structures.

Exponential Material Properties

A two-phase steel/aluminum FG plate is considered in this paper. The corresponding material parameters are: E_S=210GPa, ρ_S=7806 kg/m^3, E_{Al}=70GPa, ρ_{Al}=2707kg/m^3, and ν=0.3. The schematic sketch of the plate and its dimensions are illustrated in Fig. 1. The material properties of the FG plates are assumed to vary continuously along spatial coordinates in longitudinal or transverse directions according to an exponential law. In particular, the Poisson's ratio ν is taken as constant, while the Young's

modulus E and the mass density ρ are assumed to vary according to the following exponential functions

$$E(x_d) = E_0 e^{\beta x_d}, \qquad \beta = \frac{1}{L_d}\ln(\frac{E_1}{E_0}), \qquad \rho(x_d) = \rho_0 e^{\gamma x_d}, \qquad \gamma = \frac{1}{L_d}\ln(\frac{\rho_1}{\rho_0}), \tag{1}$$

where E_0 and ρ_0 denote the Young's modulus and the mass density for the starting face constituent, E_1 and ρ_1 are for the ending face constituent, β and γ represent the material gradient parameters for the Young's modulus and the mass density respectively, x_d (d=1,2) stands for the Cartesian coordinates, and L_d is the length parameter of the considered plate.

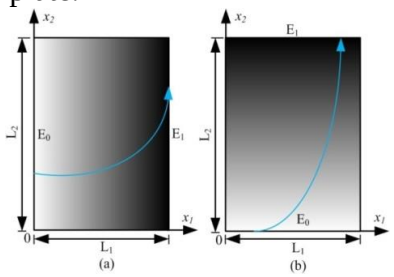

Figure 1. Coordinates and geometry of FG plates: (a) material gradation in in x_1-direction; (b) material gradation in x_2-direction

Problem Formulation and Numerical Solution Method

Based on the 2D elasticity theory, the governing partial differential equations of the steady-state elastodynamics without damping are given by

$$\sigma_{ij,j}(\boldsymbol{x}) + \omega^2 \rho u_i(\boldsymbol{x}) = 0, \tag{2}$$

where ω is the natural frequency, ρ is the mass density, u_i is the amplitude of the displacement vector, and σ_{ij} is the stress tensor. A comma after a quantity represents spatial derivatives and repeated indices denote summation.

Since the Young's modulus varies with the Cartesian coordinates while the Poisson's ratio is constant, the elasticity tensor can be described by the shear modulus $\mu(\boldsymbol{x})$ varying with the coordinates and the elasticity tensor c^0_{ijkl} for the reference homogeneous material in the form of

$$c_{ijkl}(\boldsymbol{x}) = \mu(\boldsymbol{x}) c^0_{ijkl}, \qquad \mu(\boldsymbol{x}) = \frac{E(\boldsymbol{x})}{2(1+\nu)}, \qquad c^0_{ijkl} = \frac{2\nu}{1-2\nu}\delta_{ij}\delta_{kl} + \delta_{ik}\delta_{jl} + \delta_{il}\delta_{jk}, \tag{3}$$

in which δ_{ij} is the Kronecker delta. By taking the elasostatic displacement fundamental solutions $U_{ij}(\boldsymbol{x}, \boldsymbol{y})$ as the weight function, the weak-form of the equations of motion Eq. (2) can be obtained as

$$\int_\Omega [\sigma_{jk,k} + \rho\omega^2 u_j] \cdot U_{ij} d\Omega = 0. \tag{4}$$

Application of the generalized Hooke's law $\sigma_{ij} = c_{ijkl} u_{k,l} = \mu(\boldsymbol{x}) c^0_{ijkl} u_{k,l}$ and Gauss's divergence theorem yields the following boundary-domain integral equations

$$\begin{aligned} \tilde{u}_i(\boldsymbol{y}) &= \int_\Gamma U_{ij}(\boldsymbol{x},\boldsymbol{y}) t_j(\boldsymbol{x}) d\Gamma - \int_\Gamma T_{ij}(\boldsymbol{x},\boldsymbol{y}) \tilde{u}_j(\boldsymbol{x}) d\Gamma + \int_\Omega V_{ij}(\boldsymbol{x},\boldsymbol{y}) \tilde{u}_j(\boldsymbol{x}) d\Omega \\ &+ \omega^2 \int_\Omega \frac{\rho(\boldsymbol{x})}{\mu(\boldsymbol{x})} U_{ij}(\boldsymbol{x},\boldsymbol{y}) \tilde{u}_j(\boldsymbol{x}) d\Omega. \end{aligned} \tag{5}$$

In Eq. (5), $t_i = \sigma_{ij} n_j$ is the traction vector with n_j being the components of the outward unit normal to the boundary Γ of the considered domain Ω. $\tilde{u}_i(\boldsymbol{x}) = \mu(\boldsymbol{x}) u_i(\boldsymbol{x})$ is the

normalized displacement vector and $\tilde{\mu}(\boldsymbol{x}) = \ln[\mu(\boldsymbol{x})]$ is the normalized shear modulus (Gao et al. 2008). The fundamental solutions $U_{ij}(\boldsymbol{x}, \boldsymbol{y})$, $T_{ij}(\boldsymbol{x}, \boldsymbol{y})$, and $V_{ij}(\boldsymbol{x}, \boldsymbol{y})$ are chosen as the elastostatic displacement fundamental solutions for homogeneous, isotropic and linear elastic solids with μ=1, which can be expressed as (Gao 2002b)

$$U_{ij} = \frac{-1}{8\pi(1-\nu)}[(3-4\nu)\delta_{ij}\ln(r) - r_{,i}r_{,j}], \tag{6}$$

$$\Sigma_{ijl} = c^0_{rsjl}U_{ir,s} = \frac{-1}{4\pi(1-\nu)r}[(1-2\nu)(\delta_{il}r_{,j} + \delta_{ij}r_{,l} - \delta_{jl}r_{,i}) + 2r_{,i}r_{,j}r_{,l}], \tag{7}$$

$$T_{ij} = \Sigma_{ijl}n_l = \frac{-1}{4\pi(1-\nu)r}[(1-2\nu)(n_i r_{,j} - n_j r_{,i}) + ((1-2\nu)\delta_{ij} + 2r_{,i}r_{,j})r_{,l}n_l], \tag{8}$$

$$V_{ij} = \Sigma_{ijl}\tilde{\mu}_{,l} = \frac{-1}{4\pi(1-\nu)r}[(1-2\nu)(\tilde{\mu}_{,i}r_{,j} - \tilde{\mu}_{,j}r_{,i}) + ((1-2\nu)\delta_{ij} + 2r_{,i}r_{,j})r_{,l}\tilde{\mu}_{,l}], \tag{9}$$

where $r=|\boldsymbol{x}-\boldsymbol{y}|$ is the distance from the field point $\boldsymbol{x}$ to the source point $\boldsymbol{y}$. Boundary-domain integral equations for boundary points can be obtained by letting $\boldsymbol{y}$ to the boundary Γ in Eq. (5).

There are two domain integrals emerged in Eq. (5), the first one is due to the gradation of the material properties and the other arises from the inertial effect. The radial integration method (RIM) of Gao (2002a) is employed to transform the domain integrals into boundary integrals over the global boundary. In the RIM, the normalized displacements in the domain integrals of Eq. (5) are approximated by a combination of the radial basis functions and the polynomials of the global coordinates, which has been demonstrated as the most promising one (Şimşek, and Kocatürk 2009). Then the normalized displacements $\tilde{u}_i(\boldsymbol{x})$ can be expressed as

$$\tilde{u}_i(\boldsymbol{x}) = \sum_A \alpha_i^A \phi^A(R) + a_i^k x_k + a_i^0, \qquad \sum_A \alpha_i^A = 0, \qquad \sum_A \alpha_i^A x_j^A = 0, \tag{10a, b, c}$$

where $\phi^A(R)$ is the radial basis function, α_i^A, a_i^k and a_i^0 are unknown coefficients to be determined, x_k and x_j^A denote the coordinates of the field point $\boldsymbol{x}$ and the application point A respectively. In this analysis, the following 4th order spline-type radial basis function is applied

$$\phi^A(R) = \begin{cases} 1 - 6(\frac{R}{d_A})^2 + 8(\frac{R}{d_A})^3 - 3(\frac{R}{d_A})^4, 0 \le R \le d_A, \\ 0, R \ge d_A, \end{cases} \tag{11}$$

where $R=\|\boldsymbol{x}-\boldsymbol{x}^A\|$ is the distance from the application point A to the filed point $\boldsymbol{x}$, and d_A is the support size for the application point A. The total number of the application points A is given by $N_t=N_b+N_i$ with N_b and N_i being the number of the boundary nodes and internal nodes, respectively. By choosing N_t application points A in Eqs. (10) and avoiding two coincident nodes, $\boldsymbol{\alpha}$ can be calculated by a set of linear algebraic equations as

$$\tilde{\boldsymbol{u}} = \boldsymbol{\phi}\cdot\boldsymbol{\alpha}, \qquad \boldsymbol{\alpha} = \boldsymbol{\phi}^{-1}\cdot\tilde{\boldsymbol{u}}. \tag{12}$$

Then substitution of Eq. (10a) into the domain integrals of Eq. (5) and application of RIM, the domain integrals can be transformed into boundary integrals as

$$\int_\Omega V_{ij}\tilde{u}_j d\Omega = \alpha_j^A \int_\Gamma \frac{1}{r}\frac{\partial r}{\partial n}F_{ij}^A d\Gamma + a_j^k \int_\Gamma \frac{r_{,k}}{r}\frac{\partial r}{\partial n}F_{ij}^1 d\Gamma + (a_j^k y_k + a_j^0)\int_\Gamma \frac{1}{r}\frac{\partial r}{\partial n}F_{ij}^0 d\Gamma, \tag{13}$$

$$\omega^2 \int_\Omega \frac{\rho}{\mu} U_{ij} \tilde{u}_j d\Omega = \omega^2 \frac{\rho_0}{\mu_0} e^{(\gamma-\beta)y_d} [\alpha_j^A \int_\Gamma \frac{1}{r} \frac{\partial r}{\partial n} P_{ij}^{Ad} d\Gamma + a_j^k \int_\Gamma \frac{r_{,k}}{r} \frac{\partial r}{\partial n} P_{ij}^{1d} d\Gamma$$
$$+ (a_j^k y_k + a_j^0) \int_\Gamma \frac{1}{r} \frac{\partial r}{\partial n} P_{ij}^{0d} d\Gamma], \tag{14}$$

where the relation $x_i=y_i+r_{,i}r$ is used to relate $\boldsymbol{x}$ with r. By rewriting Eq. (9) with $V_{ij} = \overline{V}_{ij} / r$, the integral functions in Eqs. (13) and (14) can be expressed as

$$F_{ij}^A = \int_0^r r V_{ij} \phi^A dr = \overline{V}_{ij} \int_0^r \phi^A dr,\ F_{ij}^1 = \int_0^r r^2 V_{ij} dr = \frac{1}{2} r^2 \overline{V}_{ij},\ F_{ij}^0 = \int_0^r r V_{ij} dr = r \overline{V}_{ij}, \tag{15a,b,c}$$

$$P_{ij}^{Ad} = \int_0^r r U_{ij} \phi^A e^{(\gamma-\beta) r_{,d} r} dr,\ P_{ij}^{1d} = \int_0^r r^2 U_{ij} e^{(\gamma-\beta) r_{,d} r} dr,\ P_{ij}^{0d} = \int_0^r r U_{ij} e^{(\gamma-\beta) r_{,d} r} dr. \tag{16a,b,c}$$

Since $r_{,i}$ in the above radial integrals is constant, then Eqs. (15b-c) can be evaluated analytically and other integrals are calculated by standard Gaussian quadrature formula. The function $\phi^A(R)$ can be expressed as a function of r, which can be done by using the following relation

$$R = \sqrt{r^2 + sr + \overline{R}^2}, \qquad s = 2 r_{,i} \overline{R}_i, \qquad \overline{R} = \left| \boldsymbol{y} - \boldsymbol{x}^A \right| = \sqrt{\overline{R} \cdot \overline{R}}, \qquad \overline{R}_i = y_i - x_i^A. \tag{17}$$

After the spatial discretization of the global boundary into quadratic boundary elements with N_b nodes, and collocating the resulting boundary integral equations at the $N_t=N_b+N_i$ boundary and internal nodes, two sets of discretized boundary integral equations are obtained, which can be expressed in matrix form as

$$\boldsymbol{H}_b \cdot \tilde{\boldsymbol{u}}_b = \boldsymbol{G}_b \cdot \boldsymbol{t}_b + \boldsymbol{V}_b \cdot \tilde{\boldsymbol{u}} + \omega^2 \cdot \boldsymbol{P}_b \cdot \tilde{\boldsymbol{u}} \qquad \text{for boundary nodes,} \tag{18}$$

$$\tilde{\boldsymbol{u}}_i = \boldsymbol{G}_i \cdot \boldsymbol{t}_b - \boldsymbol{H}_i \cdot \tilde{\boldsymbol{u}}_b + \boldsymbol{V}_i \cdot \tilde{\boldsymbol{u}} + \omega^2 \cdot \boldsymbol{P}_i \cdot \tilde{\boldsymbol{u}} \qquad \text{for internal nodes.} \tag{19}$$

The system matrices in the above equations involve boundary integrals only. The normalized displacement vector $\tilde{\boldsymbol{u}}_b$ and the corresponding traction vector $\boldsymbol{t}_b$ of the boundary nodes have the size of $2N_b$ x 1, while the normalized displacement vector of the internal nodes $\tilde{\boldsymbol{u}}_i$ has the size of $2N_i$ x 1. The normalized displacement vector $\tilde{\boldsymbol{u}}$ at all nodes has the size of $2N_t$ x 1. In Eq. (18), the matrices $\boldsymbol{V}_b$ and $\boldsymbol{P}_b$ have the dimension of $2N_b$ x $2N_t$, and in Eq. (19) the matrices $\boldsymbol{V}_i$ and $\boldsymbol{P}_i$ have the size of $2N_i$ x $2N_t$. By considering the boundary conditions, Eqs. (18) and (19) can also be written in terms of known and unknown vectors and in a more compact form as

$$\left(\begin{bmatrix} \boldsymbol{A}_b & 0 \\ -\boldsymbol{A}_i & \boldsymbol{I} \end{bmatrix} - \begin{bmatrix} \boldsymbol{V}_b \\ \boldsymbol{V}_i \end{bmatrix} \right) \begin{Bmatrix} \overline{\boldsymbol{x}}_b \\ \tilde{\boldsymbol{u}}_i \end{Bmatrix} = \omega^2 \begin{bmatrix} \boldsymbol{P}_b \\ \boldsymbol{P}_i \end{bmatrix} \begin{Bmatrix} \overline{\boldsymbol{x}}_b \\ \tilde{\boldsymbol{u}}_i \end{Bmatrix}, \tag{20}$$

where $\boldsymbol{I}$ is the identity matrix with the size of $2N_i$ x $2N_i$. The vector $\overline{\boldsymbol{x}}_b$ contains the unknown normalized displacements and unknown boundary tractions for boundary nodes, and the corresponding matrices $\boldsymbol{A}_b$ and $\boldsymbol{A}_i$, have the dimensions $2N_b$ x $2N_b$, and $2N_i$ x $2N_b$, respectively. It should be noted that the sub-columns of the matrices $\boldsymbol{V}_b$, $\boldsymbol{P}_b$ and $\boldsymbol{V}_i$, $\boldsymbol{P}_i$ corresponding to the known boundary displacement nodes should be taken as zero. In free vibration analysis, only the homogeneous system of the linear algebraic equations is needed, thus the vectors containing the known normalized boundary displacements as well as the known boundary tractions should be taken as zero. By resolving this general eigenvalue equation, the eigenvalues ω and the eigenvectors can be obtained numerically.

Numerical Examples and Discussion

The boundary conditions of the rectangular FG plates are determined by the combination of the boundary conditions on the four edges moving counter clockwise

starting from the edge x_2=0. As boundary conditions, simply supported (S), fixed (C) and free (F) boundary conditions are imposed as S: t_{x1}=0, v=0, on x_1=0; C: u=v=0, on x_1=0; F: t_{x1}= t_{x2}=0, on x_1=0 and shown in Fig. 2. The natural frequencies are all normalized by $\varpi = \omega L_2 \sqrt{\rho_{Al} / E_{Al}}$, where L_2 is the length of the analyzed plate in the x_2-direction.

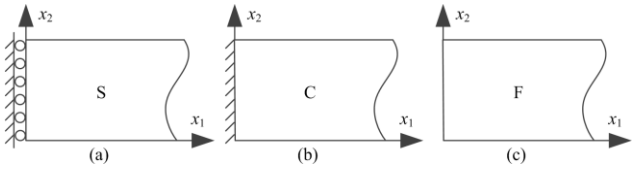

Figure 2. Different supports for FG plates (a) simply supported; (b) fixed; (c) free

To verify the accuracy of the present method, SSSS supported FG plates with aspect ratios L_1/L_2=1, 2 and 5 are studied. The first ten normalized natural frequencies are given in Table 1 and the results are compared with the FEM results by using COMSOL. The comparison shows an excellent agreement. For the FG plate with L_1/L_2=1, 20 boundary elements (N_b=40) and 81 internal nodes (N_i=81) are used and the results are compared with that of the FEM with 11081 quadratic elements. For L_1/L_2=2, N_b=60 and N_i=36 in the BEM and 20000 quadratic elements in the FEM are used. For L_1/L_2=5, N_b=120 and N_i=96 in the BEM and 13873 quadratic elements in the FEM are used. The comparison demonstrates that the present method has high accuracy even for high frequencies.

Table 1. Comparison for SSSS supported FG plates with aspect ratios L_1/L_2=1, 2, 5

Mode	L_1/L_2=1			L_1/L_2=2			L_1/L_2=5		
	N_b=40 N_i=81	FEM (11081*)	diff. %	N_b=60 N_i=36	FEM (20000*)	diff. %	N_b=120 N_i=96	FEM (13873*)	diff. %
1	1.9185	1.9207	0.11	0.9987	0.9988	0.01	0.3995	0.3995	0.01
2	1.9980	1.9975	0.03	1.9504	1.9513	0.05	0.7900	0.7901	0.01
3	2.8638	2.8637	0.01	1.9736	1.9752	0.08	1.1822	1.1826	0.03
4	3.8901	3.9026	0.32	2.2292	2.2290	0.01	1.5753	1.5756	0.02
5	3.9502	3.9503	0.00	2.7992	2.7966	0.09	1.9666	1.9689	0.11
6	4.4183	4.4118	0.15	2.9519	2.9565	0.16	1.9686	1.9690	0.02
7	4.4576	4.4579	0.01	3.5570	3.5544	0.07	2.0085	2.0083	0.01
8	5.2336	5.2355	0.04	3.9242	3.9342	0.25	2.1237	2.1225	0.05
9	5.6107	5.5932	0.31	3.9298	3.9391	0.24	2.2988	2.2976	0.05
10	5.8631	5.8875	0.41	4.0654	4.0650	0.01	2.3587	2.3622	0.15

*Number of quadratic elements

Free vibration of 2D exponential FG plates with different gradient parameters κ=0.33 and 3, where $\kappa=E_1/E_0$, gradation directions, boundary conditions (SSSS, CCCC, CFFF, FFSS, SSCC, CCFF) and aspect ratios L_1/L_2=1, 2 and 5 is then investigated. The first five normalized natural frequencies are shown in Table 2. For SSSS and CCCC supported FG plates, the frequencies for κ=0.33 and κ=3 are the same due to the double symmetry of the problem with respect to the central lines of the FG plates. For CFFF supported FG plates, the frequencies for κ=0.33 and κ=3 are the same only for the material gradation in the x_1-direction. The first five vibration modes of SSSS, CFFF and SSCC supported FG plates are presented in Fig. 3.

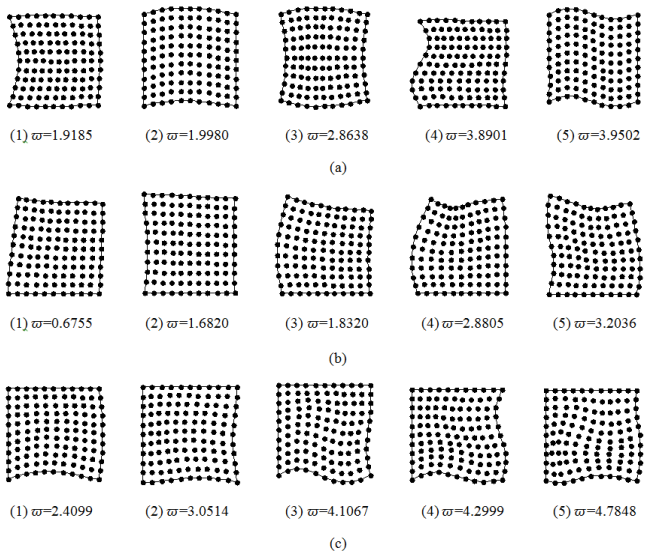

Figure 3. First five vibration modes of the FG plates with material gradation in x_1-direction, L_1/L_2=1 and κ=0.33 (a) SSSS; (b) CFFF; (c) SSCC

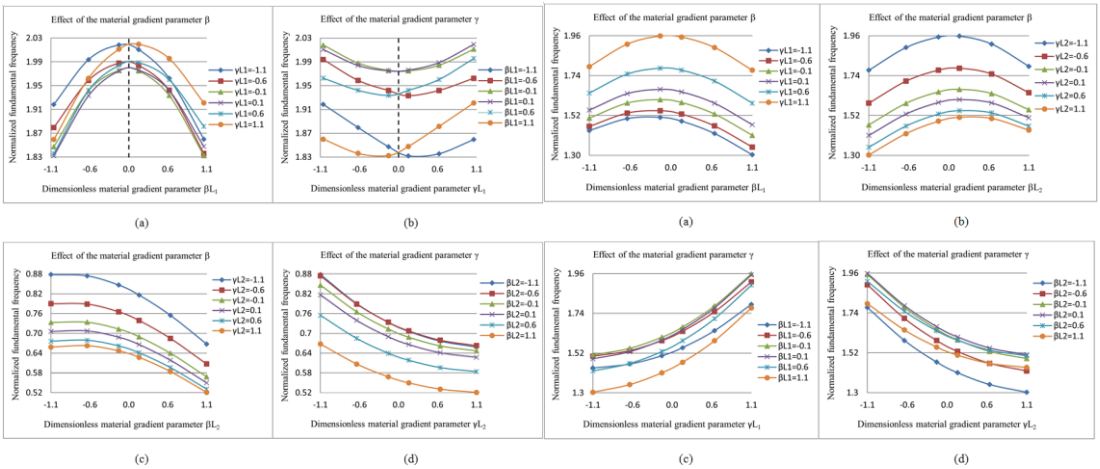

Figure 4. Effect of the material gradient parameters for FG plates with L_1/L_2=1 (a) effect of βL_1 for SSSS supported FG plates; (b) effect of γL_1 for SSSS supported FG plates; (c) effect of βL_2 for CFFF supported FG plates; (d) effect of γL_2 for CFFF supported FG plates

Figure 5. Effect of the material gradient parameter for CCFF supported FG plates with L_1/L_2=1 (a) effect of βL_1; (b) effect of βL_2; (c) effect of γL_1; (d) effect of γL_2

Fig. 4 shows the effects of the material gradient parameters β and γ on the free vibration of the FG plates. For each of both parameters six dimensionless material gradient parameters βL_d and γL_d=-1.1, -0.6, -0.1, 0.1, 0.6, 1.1 (two values with opposite signs are regarded as a pair) are considered. SSSS supported FG plates with an aspect ratio L_1/L_2=1 and a material gradation in the x_1-direction are taken as an example of doubly symmetrical FG plates with respect to their mid-lines. The normalized fundamental frequencies change with the dimensionless material gradient parameters obeying a parabolic tendency as shown in Fig. 4(a). For a fixed material gradient parameter βL_1, each pair of γL_1 intersects at the value for homogeneous case and achieves the highest frequency. A decreasing absolute value of γL_1 decreases the

fundamental frequencies. However, the material gradient parameter γL_1 has a totally opposite effect on the natural frequencies which can be observed from Fig. 4(b). For CFFF supported FG plates with a material gradation in the x_1-direction, the influences of the material gradient parameters on the free vibration are the same as that of the doubly symmetrical (with respect to the mid-lines) FG plates. For a material gradation in the x_2-direction as shown in Fig. 4(c), an increasing dimensionless parameter βL_2 decreases the fundamental frequencies, while the normalized natural frequencies decrease with the increase of the dimensionless material gradient parameter γL_2. The influence of the material gradient parameter γL_2 is similar to that of βL_2 but with an opposite slope.

Fig. 5 presents the normalized fundamental frequencies versus the dimensionless material gradient parameters for asymmetrical CCFF supported FG plates with an aspect ratio L_1/L_2=1. To investigate the effect of the aspect ratio on the free vibration of FG plates, the normalized natural frequencies versus the dimensionless material gradient parameters with aspect ratios L_1/L_2=1, 2 and 5 are shown in Fig. 6. Generally, an increasing aspect ratio decreases the normalized natural frequencies, as shown in Fig. 6(a) for the SSSS supported FG plates with a material gradation in the x_1-direction. However, for CFFF supported FG plates, an opposite tendency is observed. As an example, the corresponding results for CFFF supported FG plates with a material gradation in the x_2-direction are shown in Fig. 6(b).

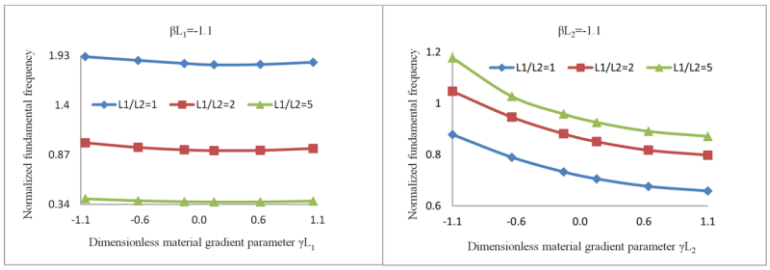

(a) (b)

Figure 6. Effect of the aspect ratios L_1/L_2=1, 2, 5 on the normalized fundamental frequencies of (a) SSSS supported FGM plates with material gradation in x_1-direction; (b) CFFF supported FG plates with material gradation in x_2-direction

Conclusions

In this paper, a meshfree boundary-domain integral equation method for free vibration analysis of two-dimensional FG plates is presented. An exponential law is used to describe the continuous material gradation either in longitudinal or transverse directions. The effects of the material gradient parameters, gradation directions, aspect ratios and boundary conditions on the free vibration of the FG plates are investigated in details by numerical examples. The numerical examples demonstrate that the present method has fast convergence, high efficiency and accuracy.

References

Nardini, D., Brebbia C. A. (1983), A new approach to free vibration analysis using boundary elements. Applied Mathematical Modelling, 7(3), pp. 157-162.

Gao, X. W. (2002), The radial integration method for evaluation of domain integrals with boundary-only discretization. Engineering Analysis with Boundary Elements, 26(10), pp. 905-916.

Albuquerque, E. L., Sollero, P., Fedelinski, P. (2003), Free vibration analysis of anisotropic material structures using the boundary element method. Engineering Analysis with Boundary Elements, 27(10), pp. 977-985.

Albuquerque, E.L., Sollero, P, Portilho de Paiva W. (2006), The radial integration method applied to dynamic problems of anisotropic plates. Communications in Numerical Methods in Engineering, 23(9), pp. 805-818.

Ekhlakov, A., Khay, O., Zhang, Ch. (2010), Effects of the material gradation on the SIFs of a crack in a 2-D FGM plate under thermal shock. Proceedings in Applied Mathematics and Mechanics, 10(1), pp. 111-112.

Ekhlakov, A. V., Khay, O. M., Zhang, Ch., Sladek, J., Sladek, V. (2012), A BDEM for transient thermoelastic crack problems in functionally graded materials under thermal shock. Computational Materials Science, 57, pp. 30-37.

Gao, X. W., Zhang, Ch., Sladek, J., Sladek, V. (2008), Fracture analysis of functionally graded materials by a BEM. Composites Science and Technology, 68, pp. 1209-1215.

Gao, X. W., Davies, T. G. (2002), Boundary Element Programming in Mechanics. Cambridge University Press.

Golberg, M. A., Chen, C. S., Bowman H. (1999), Some recent results and proposals for the use of radial basis functions in the BEM. Engineering Analysis with Boundary Elements, 23, pp. 285-296.

Şimşek, M., Kocatürk, T. (2009), Free and forced vibration of a functionally graded beam subjected to a concentrated moving harmonic load. Composite Structures, 90, pp. 465-473.

Table 2. First five normalized natural frequencies of SSSS, CCCC, CFFF, FFSS, SSCC and CCFF supported FG plates

BC	GD	κ	L_1/L_2=1					L_1/L_2=2					L_1/L_2=5				
			1st	2nd	3rd	4th	5th	1st	2nd	3rd	4th	5th	1st	2nd	3rd	4th	5th
	x_1	0.33	1.9185	1.9980	2.8638	3.8901	3.9502	0.9987	1.9504	1.9736	2.2292	2.7992	0.3995	0.7900	1.1822	1.5753	1.9666
SSSS		3	1.9210	1.9986	2.8644	3.9020	3.9451	0.9987	1.9504	1.9736	2.2292	2.7992	0.3995	0.7900	1.1822	1.5753	1.9666
	x_2	0.33	1.9213	1.9973	2.8641	3.8997	3.9464	0.9462	1.9185	1.9968	2.2599	2.8659	0.3758	0.7549	1.1387	1.5278	1.9184
		3	1.9213	1.9973	2.8641	3.8997	3.9464	0.9462	1.9185	1.9968	2.2599	2.8659	0.3758	0.7549	1.1387	1.5278	1.9184
	x_1	0.33	4.0353	4.0712	4.5259	5.8049	6.3136	2.6543	3.6359	3.6661	3.9935	4.1453	2.0916	2.4151	2.8717	3.3908	3.4700
CCCC		3	4.0367	4.0747	4.5251	5.8077	6.3019	2.6543	3.6359	3.6661	3.9935	4.1453	2.0916	2.4151	2.8717	3.3908	3.4700
	x_2	0.33	4.0381	4.0713	4.5257	5.8067	6.3011	2.6569	3.6805	3.6991	3.9968	4.1827	2.1154	2.4354	2.8881	3.4016	3.5159
		3	4.0381	4.0713	4.5257	5.8067	6.3011	2.6569	3.6805	3.6991	3.9968	4.1827	2.1154	2.4354	2.8881	3.4016	3.5159
	x_1	0.33	0.6755	1.6820	1.8320	2.8805	3.2036	0.8326	1.5934	1.7656	1.8556	2.1765	0.9178	1.0904	1.5290	1.7364	1.7956
CFFF		3	0.6753	1.6824	1.8328	2.8844	3.1974	0.8326	1.5934	1.7656	1.8556	2.1765	0.9178	1.0904	1.5290	1.7364	1.7956
	x_2	0.33	0.8782	2.0385	2.1389	3.0845	3.2308	1.0468	1.7526	2.1232	2.1783	2.4654	1.1336	1.2565	1.6857	1.8286	1.9649
		3	0.5208	1.3455	1.5414	2.8038	3.0062	0.6565	1.3411	1.4365	1.5979	1.9382	0.7291	0.9418	1.3367	1.4113	1.4440
	x_1	0.33	1.4112	2.4668	2.7163	2.9319	3.6889	1.0305	1.2060	1.8981	2.1627	2.7168	0.3046	0.6738	0.9972	1.0731	1.2833
FFSS		3	1.0375	2.1785	2.7945	2.9075	3.7173	0.7315	1.3365	1.8173	2.1102	2.6000	0.2554	0.6386	0.9571	1.1028	1.2608
	x_2	0.33	1.0373	2.1783	2.7933	2.9074	3.7170	0.7630	1.1495	1.7493	1.9655	2.6416	0.2918	0.6346	0.8182	0.9842	1.1337
		3	1.4118	2.4670	2.7181	2.9320	3.6896	0.9299	1.3978	1.9427	2.3003	2.6278	0.0002	0.2597	0.6381	1.0249	1.2475
	x_1	0.33	2.4099	3.0514	4.1067	4.2999	4.7848	1.8686	2.2288	2.4994	3.1320	3.4424	1.7363	1.7862	1.8858	2.0292	2.1114
SSCC		3	2.0816	2.8309	3.9397	4.1037	4.6979	1.7956	2.1908	2.4108	3.1268	3.3633	1.7344	1.7853	1.8755	2.0238	2.0933
	x_2	0.33	2.0816	2.8310	3.9375	4.1062	4.6984	1.5432	2.0756	2.3047	2.9699	3.3633	1.4124	1.4557	1.5877	1.8128	2.0401
		3	2.4102	3.0517	4.1070	4.2998	4.7849	2.0485	2.3943	2.7059	3.2819	3.5138	1.9923	2.0226	2.1330	2.2827	2.3887
	x_1	0.33	1.4373	1.9425	2.2423	3.5871	4.0334	1.0574	1.7672	1.8869	2.3545	2.6623	0.9503	1.3496	1.7264	1.8013	1.8315
CCFF		3	1.7702	2.4659	2.6311	3.8513	4.2927	1.2823	1.8594	1.9299	2.4445	2.7816	1.0063	1.3726	1.7251	1.7993	1.8358
	x_2	0.33	1.7701	2.4656	2.6287	3.8545	4.2840	1.3241	2.1588	2.2398	2.6790	2.8262	1.1772	1.5222	1.9647	2.1653	2.2181
		3	1.4394	1.9431	2.2459	3.5852	4.0440	1.0390	1.4625	1.6019	2.1521	2.6256	0.7998	1.2200	1.4207	1.4435	1.4728

BD: boundary condition; GD: gradation direction